High temperature difference in a new flexible thermoelectric bismuth telluride microgenerator

G Moiroux, C Tur, Daniel Bourgault, Jean-Luc Garden

High temperature difference in a new flexible thermoelectric bismuth telluride microgenerator

G. Moiroux [1,2], C. Tur[1,2], D. Bourgault[1,2], J.-L. Garden[1,2]

[1]*Univ. Grenoble Alpes, Institut Néel, F-38042 Grenoble, France.*

[2]*Centre National de la Recherche Scientifique / Institut Néel, 25 Avenue des Martyrs, BP 166, 38042 Grenoble Cedex 9, France*

Corresponding author: G.Moiroux email : gael.moiroux@neel.cnrs.fr

Abstract

We present new microTEGs based on doped Bi_2Te_3 thin films deposited on polyimide membrane able to operate under a temperature difference as high as 280 K. We developed two microTEGs with different designs to obtain the lowest internal resistance possible. The thermoelectrical properties coupled to the low contact resistance lead to an open circuit voltage of 64 mV and a maximum output power of 36 µW under a temperature difference of 206 K. Such high temperature difference cannot be obtain in bulk commercial TEG systems; it is maintained without heat sink but only using a copper ring supporting a thin polyimide membrane. These thermoelectric devices deposited on suspended polyimide membranes open new ways for waste heat applications, in particular by direct mechanical and thermal contact with hot sources.

Keywords: Flexible thermoelectric generator, thermoelectrical thin film, bismuth telluride, dc magnetron sputtering, contact resistance

1. Introduction

Thermoelectricity is very attractive because it can convert heat energy directly into electrical energy by Seebeck effect and reversibly electricity can remove or produce heat by Peltier effect. Thermoelectric (TE) harvesting has become a challenge sought by many industrials particularly in the field of microelectronics engineering. Although there has been significant progress in manipulating new formulations and nano-structuring existing compounds [1], little work has been undertaken on devices development for micro-generation or thermoelectric microcooling [2-4]. This field of application represents a crucial interest for the world of autonomous electronic microsystems which requires local sources of renewable energy [5,6]. Personal networks (nomadic connected objects), consisting of microcontrollers, sensors and wireless communication chips, are typical applications for which thermoelectric energy recovery could be used [7,8].

Bi_2Te_3-based materials are widely used for Peltier cooler and power generation applications near room temperature because of the high figure of merit $ZT = \frac{S^2}{\rho\kappa}T$, where S, ρ, and κ are the Seebeck coefficient, electrical resistivity, and thermal conductivity of the material, respectively, and T is the

temperature. $Bi_{0.5}Sb_{1.5}Te_3$ and $Bi_2Te_{2.7}Se_{0.3}$ have been recognized as the best p-type and n-type TE materials due to the combination of high power factor ($PF = \frac{S^2}{\rho}$) and low thermal conductivity [9]. Several techniques have been exploited to deposit Bi_2Te_3-based thin films, such as molecular beam epitaxy (MBE) [10, 11], magnetron sputtering [12-15], flash evaporation [16], pulsed laser deposition (PLD) [17,18], Metal Organic Chemical Vapor Deposition (MOCVD) [19], electrochemical deposition [20-22] and ion beam sputtering [23,24].

Micro-thermoelectrical generators (microTEG) and nano-thermoelectrical generators (nanoTEG) have emerged these last decades for which power output of few tenths of µW to few µW can be obtained [25-37]. The performances depend on TE properties and also on internal resistances due to thin films geometry and specific contact resistance between metallic junctions and n and p-type legs. For microTEGs, there are two types of configuration: a perpendicular configuration (cross-plane) for which the temperature gradient along the film thickness is very low, and a planar configuration (in-plane) for which the temperature gradient is greater but with much higher internal resistances. For this last configuration, the substrate in parallel with the TE film plays a predominant role on the temperature difference that can be obtained along the TE device. In addition, the thermal coupling between the heat source and the TE device is never optimized and the temperature difference obtained along the TE device is currently considerably reduced. Some devices have been developed on polyimide substrates which have particularly interesting mechanical and thermal properties [38-47]. Among these works, Kato *et al.* developed thermoelectric legs on long polyimide tapes (several square centimeters and 20 couples) in which an output power of around 100 µW is generated through a temperature difference of 130 K [48].

To date, bulk or thin bismuth telluride modules are not usable over the entire temperature range with a high figure of merit (typically 300K 550K) because the temperature differences are only few tens of degrees with the requirement of integrating a heat sink on the systems. In this work, we present a new concept of microgenerator based on bismuth tellurium thin films deposited on a thin polyimide membrane allowing to work under temperature differences of 280K and without large heat sink.

2. Design and microfabrication process

i) Deposition of doped Bi_2Te_3

The performances of a TEG (efficiency, maximum output power) depend on the dimensionless figure of merit. The best-known TE materials, like Bi_2Te_3-based materials have a figure of merit close to 1 although certain works report on higher values [1,49,50] which are still difficult to reproduce. The films were deposited using a home-made dc magnetron sputtering vacuum chamber. 50 mm diameter hot pressed targets were used with $Bi_2Te_{2.7}Se_{0.3}$ stoichiometric compositions for n-type and $Bi_{0.5}Sb_{1.5}Te_3$ for p-type materials. The substrate used was a polyimide membrane (Upilex©S) of 25 µm thick suspended on a copper ring of 28 mm in diameter and 2 mm in thickness. n-type and p-type films are annealed in an oven under Ar at atmospheric pressure during two hours at 523K before the deposition of a layer of Ni/Pt for electrical contacts. Such optimal annealing conditions have been determined in previous studies for the crystallization of n-type and p-type films. [51]. Pressure in the chamber before deposition was lower than 10^{-6} mbar. The sputtering parameters such as argon pressure, deposition time, plasma power and substrate-target distance are indicated in table 1. n-type ($Bi_2Te_{2.7}Se_{0.3}$) and p-

type TE ($Bi_{0.5}Sb_{1.5}Te_3$) thin films with these compositions have already been used in the development of different TEGs and nano-TEGs [30,31].

	Argon pressure (mbar)	Deposition time (min)	Plasma power (W)	Substrate-target distance (cm)
Usual deposition parameters	1.5×10^{-2}	40 to 80 (1 to 2 µm)	10	10

Table 1 : Description of the sputtering parameters for devices C4 and M1.

Seebeck coefficient, *S*, and electrical resistivity, ρ, of the films are measured with home-made devices described in Ref. [13]. Electronic transport properties as well as the PF of n-type and p-type bismuth telluride thin films deposited on polyimide are given in table 2.

For both films, the variation of the normalized Seebeck coefficient and electrical resistivity as a function of temperature from 300K to 360K is shown in Figures S1 and S2 in the supplementary material.

Table 2 also gives quantitative compositions of n-type and p-type films analyzed by EDS performed with an environmental scanning electron microscope (ESEM FEI Quanta 200). Three different regions of each film were analyzed with the same conditions (accelerating voltage, beam current, magnification, acquisition time). n-type and p-type films composition were respectively $Bi_{2.1}Te_{2.65}Se_{0.25 \pm 0.05}$ and $Bi_{0.55}Sb_{1.6}Te_{2.85 \pm 0.05}$.

The phase structures of n-type and p-type films were investigated by XRD analysis. The main phase of the film is $Bi_{0.5}Sb_{1.5}Te_3$ with diffraction peaks indexed based on JCPDS n°. 49-1713. Films crystallized into a rhombohedral structure with space group R3m and lattice parameters a and c are respectively 4.296 Å and 30.484 Å. The peak (015) is the dominant diffraction peak, suggesting no preferred growth orientation. For n-type film diffraction peaks reveal that the main phase is $Bi_2Te_{2.7}Se_{0.3}$ (JCPDS n°. 50-0954) with lattice parameters a and c respectively of 4.286 Å and 30.176 Å.

	Seebeck coefficient, S (µV/K)	Power factor, PF ($W.m^{-1}K^{-2}$)	Electrical resistivity, ρ (Ω.m)
$Bi_{0.55}Sb_{1.6}Te_{2.85}$ (type p)	+255	6.9×10^{-4}	9.5×10^{-5}
$Bi_{2.1}Te_{2.65}Se_{0.25}$(type n)	-159	1.9×10^{-3}	1.3×10^{-5}

Table 2 : Compositions and electronic transport properties for n-type and p-type films.

According to the thermal conductivities of 0.55W/mK and 0.79 W/mK measured in previous works [52] for respectively n-type and p-type films, figure of merit ZT are respectively 1 and 0.25.

ii) Design

A TEG not only consists of n-type and p-type thermoelectric elements assembling. Geometrical 3D dimensions with substrate and heat sink must be taken account. Hence, the effective figure of merit, given by $ZT = \frac{S^2}{RK}T$, where *R* and *K* are respectively the resistance and the conductance, is more appropriate to consider the TEG performances. The total resistance of the device *R* includes electrical

contacts, and *K* the thermal coupling between the two thermal baths. The strategies to design a TEG with a maximal efficiency, or a TEG with a maximal output power, are in general slightly different. When heat sources to be converted are present in infinite quantities, a maximal output power is desirable, while highly efficient TEGs are more suitable when it is difficult to harvest small heat sources of low temperature bath. The maximum output power that can be generated by a TEG is given by $Pmax_{out} = \frac{V_{open}^2}{4R_{int}} = \frac{S^2(\Delta T)^2}{4R_{int}}$ when the load resistor is equal to the internal resistance of the TEG ($R_L = R_{int}$). V_{open} is the voltage at the boundaries of the TEG in open circuit conditions (or equivalently for an infinite value of the load resistor), in presence of a temperature difference ΔT (see Figure 1)

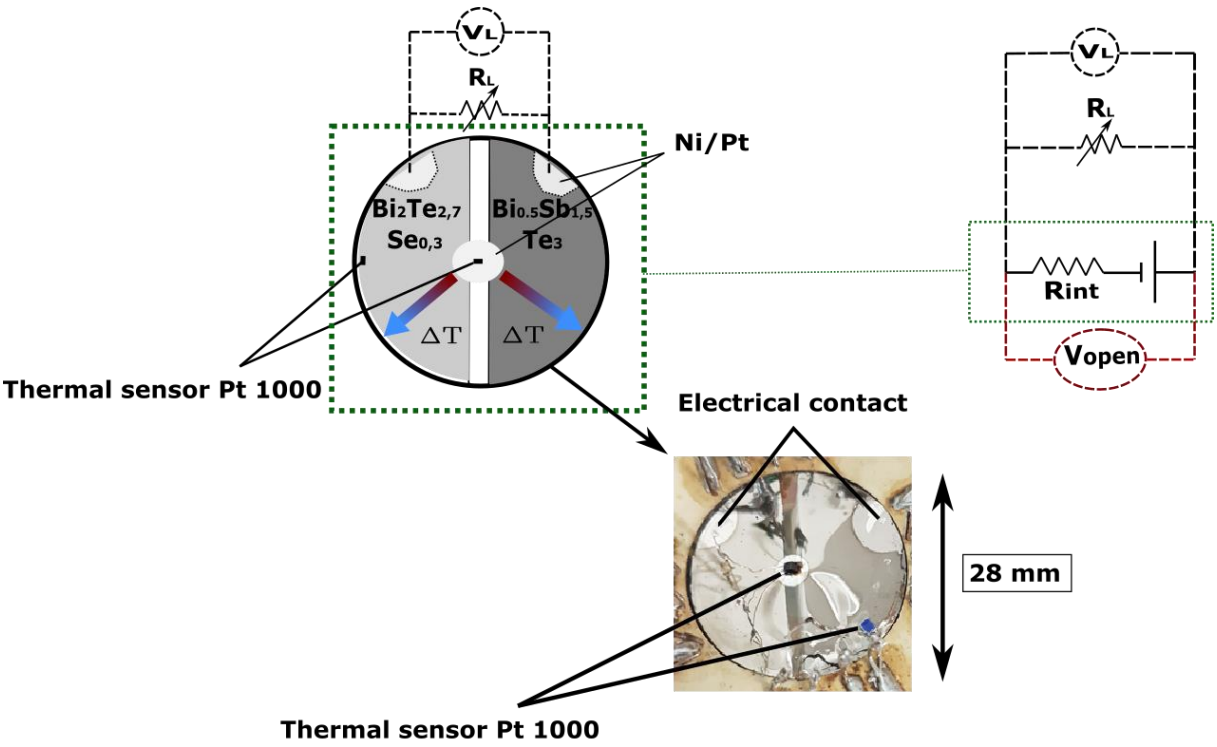

Figure 1 : Schematic view, picture and equivalent electric circuit of the device under measuring conditions.

Schematic view and picture of the device are presented in figure 1, with the corresponding electrical equivalent circuit. The two hemispheric bismuth telluride TE thin films are connected using a small disk of nickel/platinum film. Two electrical contacts located at the periphery of the device ensure the voltage measurement of the n-p junction. A temperature difference between the center and the thermal sink is generated by a heater glued on the back side of the polyimide substrate and located at the central part of the TEG (cylindrical symmetry). In order to maximize the generated electrical power, the temperature difference as well as the effective power factor have to be the highest possible. For the establishment of a maximum temperature difference, how heat is supplied at the hot junction of the TEG is an important issue. Moreover, it is crucial that the TE materials used for the TEG have their highest values of power factor in the operating temperature range. For a given value of the materials Seebeck coefficients and a given geometry of the TEG, this means that internal resistance has to be the lowest possible. Here we have developed the micro-TEG according to these requirements. Firstly, the Bi_2Te_3-based (n-type and p-type) materials show high TE transport electronic properties upon the

process and deposition conditions used for their elaboration (see table 2). A high temperature limit is of 573 K. Above this temperature bismuth telluride TE performance decreases, principally due to a change of the composition and consequently to a change of the carrier concentration. [52].

The internal resistance R_{int} of a device is the sum of the contact resistance $R_{contact}$ and the thermoelectric thin-film resistance R_{thermo} of type n and type p. The contact resistance $R_{contact}$ is function to the areal contact resistance ρ_c expressed in Ω cm^2 and the contact area S_{area} between the metal and the thermoelectric thin film ($\rho_c = R_{contact} * S_{area}$). The term R_{thermo} is function to the electrical resistivity of the thin films and of the geometric ratio length / cross section.

Two devices (C4 and M1) have been realized (Table 3) to test different internal resistances. Principal differences between both concern the Ni/Pt contact geometry: For C4 device, a small contact surface of 50 mm^2 has been chosen as it can be observed on the picture of Figure 1. For M1device, this surface was significantly increased by a factor of around 10 in view to reduce contact resistances. This parameter is crucial since it's greatly influences the overall power generated by the microsensor.

In addition, there is a difference in the thickness of the film deposition with 1 µm for C4 and 2 µm for M1 TEG. A detailed drawing showing the differences in contact geometry is shown in figure S2 in supplementary material for a better understanding of the devices design.

The smallest contact surfaces are those at the level of the hot junctions because of the smaller available surface at the center of the membrane due to the radial symmetry. However, when we estimate the theoretical resistance of the C4 device considering only the electrical resistivity contributions of the n-type and p-type thin films, we find a value of 51.6 Ω. This value is about 20% lower than the total internal resistance R_{int} ($64.6\,\Omega$). For the second TEG M1 with larger surface contact, the measured internal resistance of 28.0 Ω is very close to the theoretical value (25.8 Ω). In this case, contact resistances are estimated to contribute less than 8% of the total value.

	Thin films thickness (µm)	Ni/Pt contact surface (mm^2)	Measured internal resistance (Ω)	Theoretical resistance (Ω)
C4 TEG	1	50	64.6	51.6
M1 TEG	2	500	28.0	25.8

Table 3: Films thickness, contact surface and resistances for C4 and M1 TEG.

TE films of thicknesses between 1 µm to 2 µm are deposited on a polyimide suspended membrane (Upilex©S) of 25 µm thick. The polyimide has been chosen for three reasons: firstly, it is not deteriorated till 573K, even under air. Secondly, its low thermal conductivity (about 0.3 W/m.K) lower than that of Bi_2Te_3 materials (1W/m.K) allows thicknesses such as to preserve its mechanical properties, while avoiding highly parasitic heat losses. For a sake of comparison, in terms of thermal conductance, 25 µm of polyimide is equivalent to 2.5 µm of SiN [30] and to 0.125 µm of doped Si [28]. Thirdly, the polyimide membrane flexibility allows direct thermal and mechanical coupling of the hot junctions (in the membrane center) to external heat sources of any type (see section 4 "Practical use"). The in-plane configuration permits energy harvesting in high temperature difference for a relatively low amount of heat captured at the hot junctions. Hence, by comparison with cross-plane configurations, there is no need to cool the cold source in order to evacuate the heat-flux (fans, water circulation, etc….). In M1 device a supplied thermal power of only 500 mW leads to a temperature difference of about 300 K between the hot and cold junctions. It should be mentioned that this high

thermal difference has been obtained under air where convection is predominant (see Figure 2). The total heat exchange of the device is close to 1.6 mW/K whatever the ΔT range.

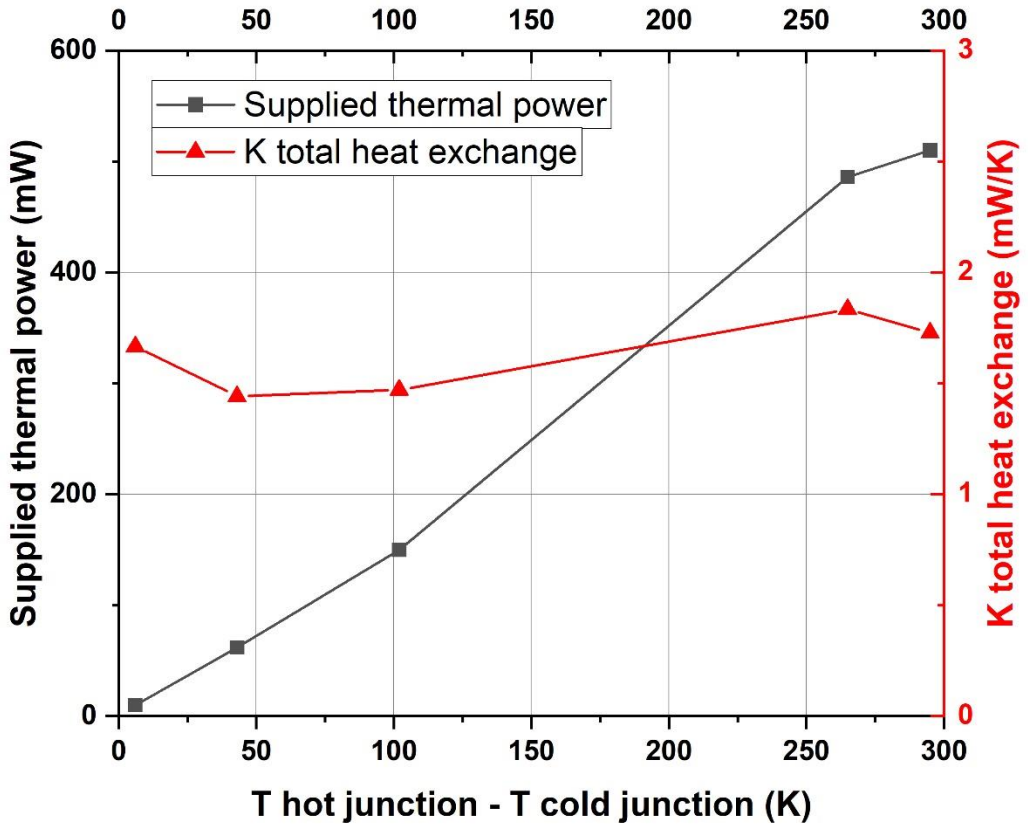

Figure 2 : Evolution of the supplied thermal power and the heat exchange with the temperature difference for M1 TEG.

3. Power generation performance

i) Experimental method of measurement

The input power is supplied at the center of the membrane by a platinum RTD Heraeus element (1000 Ω). The Pt1000 is glued at the backside of the membrane at the level of central Ni/Pt contact (see the 4 mm in diameter disk of Ni/Pt in figure 1). The Pt1000 is used here only as a heater. Current supplied in the Pt1000 is measured in the same time as the voltage across the resistor (four wires method) giving precisely the supplied power. Two other Pt1000 sensors are glued directly on the hot and cold junctions of the micro-TEG as shown in the picture of figure 1.

The TEG is embedded in a sample holder containing four series of four pins connected to thin copper wires. The Pt1000 thermometers are measured in four wires mode with two voltmeters (Prema 5017). The hot (Th) and cold (Tc) junction temperatures are permanently recorded. In all our experiments, the temperature Tc does not change more than $\pm$ 1 K due to room temperature

regulation. As mentioned before, the heat exchange coefficient between the central part of the membrane and the surrounding is of about 1.6 mW/K (mean value of the heat exchange coefficient in figure 2). Under these conditions, we verified that the power supplied by the Th-thermometer is negligible. On the 30 KΩ-range, a current of 100 µA in the Pt1000 induces a power of about 10 µW giving rise to a temperature elevation of about 6 mK, well below the values of the temperature differences (between 200K and 300K) supplied for the measurements. The supplied power of the heater is in the range of few mW to 500 mW. In this case, the current is imposed via a current source (AOIP 8310) and the voltage (Prema 5017) across the heater is permanently measured giving precisely the power supplied at the hot junction. Four copper wires are connected using gold spring contacts to measure the voltage difference across the TEG and the internal resistance (see figure 1). The data are recorded using a Schlumberger SI 7063 voltmeter. Since the two cold junctions are located on the heat bath, their temperatures are identical, and there is no significant supplementary parasitic electromotive force at the level of these contact pins. From these two spring gold contact pins, two other wires are used to connect the TEG to a rheostat (see scheme in figure 1). The value of the load resistor (R_L) is varied between 0.1 Ω to 100 KΩ. When varying the R_L, the voltage across the TEG is continuously measured.

ii) Open voltage characteristics

In a first series of measurements, the power is supplied at the level of the hot junction, and the voltage difference (V_{open}), across the TEG in open circuit condition, as well as the corresponding temperature difference are measured. Figure 3 shows the experimental data $V_{open} = f(\Delta T)$ plotted with blue and black points respectively for C4 and M1 TEGs.

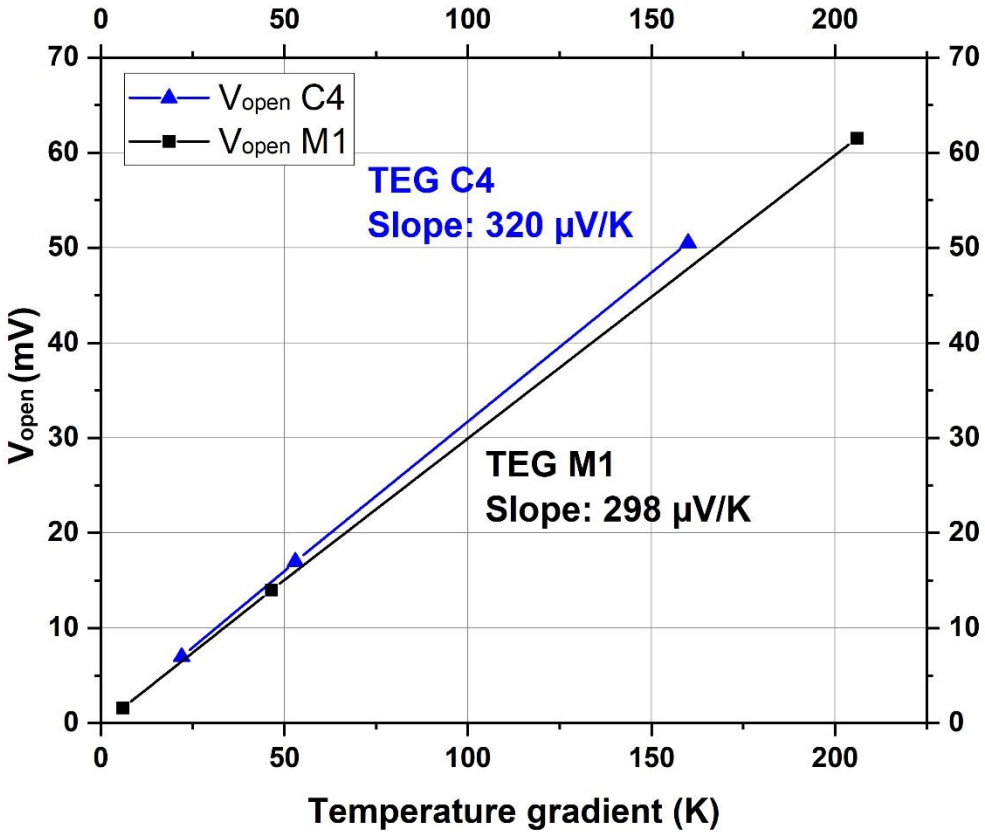

Figure 3 : Evolution of the voltage V_{open}(open circuit condition) with the temperature gradient for C4 (in blue) and M1 (in black) TEGs.

The open voltage variation for different temperature gradients is linear for both TEGs. The slope gives the average value of the Seebeck coefficient for one p-n junction on the whole temperature gradient range. The average *S* values for C4 and M1 TEGs are respectively 320 and 298 μV/K. These values are slightly lower than the theoretical Seebeck coefficient of a n-p junction according to the intrinsic Seebeck coefficients shown in table 1 ($S_{theoretical}$ = 255 + 159 = 414 μV/K). This difference is due to the fact that the intrinsic *S* coefficients were measured at room temperature whereas the average *S* values were determined with temperature varying from 300K up to 460K (for C4) and 510K (for M1). As shown in figure S2, the p-type Seebeck coefficient is optimum for a temperature of 340K before decreasing from this temperature. This behavior is classical for bismuth telluride compounds. In the literature, according to the preparation of the samples and the annealing carried out, the Seebeck coefficient decreases by 25 to 33% from a temperature between 330K and 425K for the n-type and the p-type [53-55]. We can notice that the Seebeck coefficient is not affected by the thickness of the TE thin films.

iii) Power generation

In a second series of experiments, the TEG is connected to a variable load resistor under a constant thermal gradient such as described above. When the load resistance is much higher than the internal resistance ($R_L \gg R_{int}$), there is merely no current circulating in the loop and V_L is equal to its open-circuit value ($V_L \sim V_{open}$). Inversely, when R_L is negligible with respect to the internal resistance ($R_L \ll R_{int}$) the maximal value of the current (current in short-circuit condition) circulates in the loop. Under these two particular conditions, there is no available generated power from C4 and M1 TEGs as shown in respectively figures 4a and 4b.

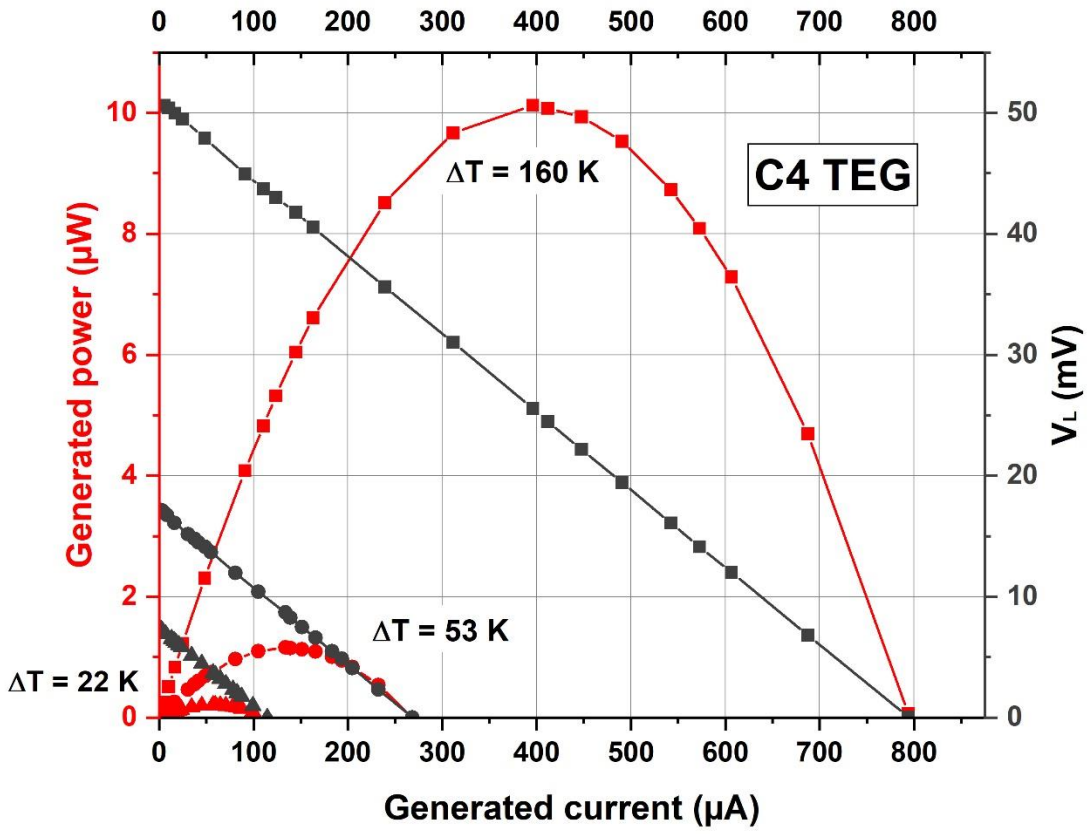

Figure 4a : Voltage difference V_L (in black) and generated power (in red) recorded for C4 TEG versus generated current for different temperature gradients.

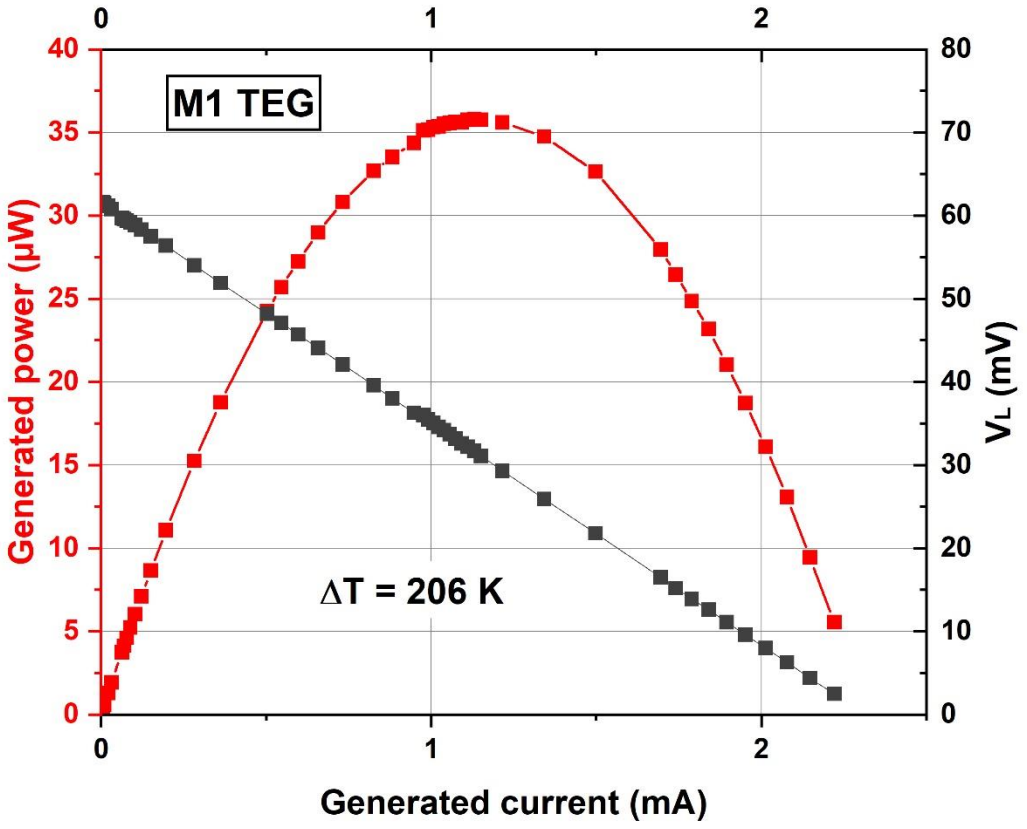

Figure 4b : Voltage difference V_L (in black) and generated power (in red) recorded for M1 TEG versus generated current for a temperature difference of 206 K.

In figures 4a and 4b, experimental data are presented for the two TEGs C4 and M1. The left scale shows the generated power ($P_{out} = V_L \times i$) as a function of the current in the circuit (see the equivalent circuit in figure 1). The right scale shows the voltage across the load resistor as a function of the same current ($V_L = f(i)$). The voltage difference (V_L) decreases linearly from V_{open} up to 0 when the R_L varies from 100 kΩ up to 0.1 Ω. The slope of the fitted straight lines gives R_{int} while the ordinate at the origin gives V_{open}. When the load resistance is much higher than the internal resistance ($R_L \gg R_{int}$), there is merely no current circulating in the loop and V_L is equal to its open-circuit value ($V_L \sim V_{open}$). The maximum harvesting power is $P_{out} = \frac{{V_L}^2}{R_L} = \frac{V_{open}^2}{4R_L}$ when the load resistance is equal to the internal resistance.

To compare C4 and M1 devices, figure S3 in supplementary material shows measured power and fitted values obtained from the formula $Pmax_{out} = \frac{V_{open}^2}{4R_{int}} = \frac{S^2(\Delta T)^2}{4R_{int}}$ according to the Rint measured and S obtained in figure 3 (S=320 and 298 μV/K for respectively C4 and M1 devices) are plotted. This graph compares the power for the same temperature difference and shows that the generated power performance is higher for M1 depending on the internal resistance.

The M1 TEG has a maximum electrical power of about 36 μW upon a constant differential temperature of 206 K, a current of 1.15 mA ($R_{int} = R_L$), with an open circuit voltage of 64 mV without the need to cool the cold junctions. These values may be of interest for low power applications. In taking the sensitive surface of the TEG, i.e. the surface of the suspended membrane delimited by a

diameter of 18 mm over which the temperature difference is converted, the maximum power by surface units is of 14.2 µW/cm^2. For a maximum possible temperature difference of 280 K (i.e. the center of the membrane being at Th = 573 K) the available maximum power could be of 63 µW (~ 25 µW/cm^2). The power output achieved with our device at ΔT=206 K is higher than those found in other planar devices for which low temperature difference can be applied [28,30]. However, such values remain lower than those obtained by Davila et al. [27]. A power output of 1.4mW/cm^2 has been obtained for a ΔT of 300K in a complex device based on successive linkages of multiple Si nanowire arrays.

Ageing tests were carried out on device M1 subjected to a temperature difference of 150K for 8 hours. The curve showing this $\Delta V/\Delta T$ evolution can be seen in figure S4 in supplementary material. After eight hours the decrease of the Seebeck coefficient of the junction is less than 2%. More complete tests at temperature differences close to 210K are planned in the near future.

The micro-TEG of the C4 type is less performant with a maximum recorded power around 10 µW only, an internal resistance of 64.6 Ω, an open circuit voltage of 51.3 mV, and a current of 400 µA. In this later case, the internal resistance was too high due to the presence of parasitic interface resistances, as well as a lower film thickness. For this device, the power output recorded for different ΔT follows the expected parabolic law P α ΔT^2.

4. Practical use

The 25 µm thick polyimide membrane is flexible enough to adapt its shape in the center of the micro-TEG to solid surfaces. Moreover, it is robust enough to support an important mechanical pressure (well above 10 bars) on the hot junction with surface close to 10 mm^2 in our configuration. As a consequence, hot conductive rods may supply directly by strong mechanical contact an amount heat from an external source directly to the hot junction of the TEG (see Figure 5). The deformation of the membrane containing the thin films at this location permits heat transfer without loss. In other words, an external source of temperature T_S is theoretically able to heat the hot junction to approximately the same temperature if the rod is conductive enough (copper rod for example).

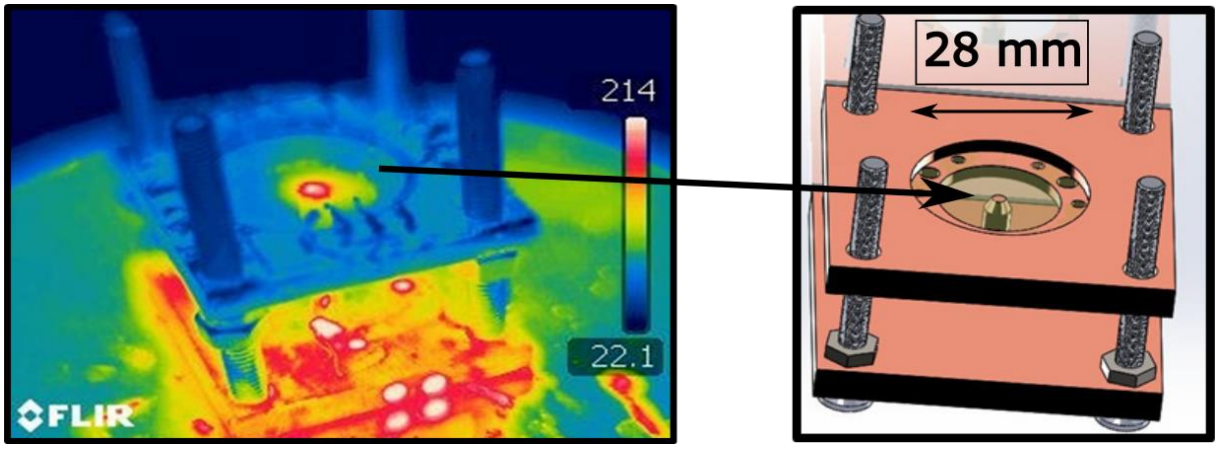

a) b)

Figure 5 : Thermal view of the device for a temperature gradient of around 200K (a) and associated scheme (b)

In order to test this specificity of our TEG device, the center of one micro-TEG is put in contact with a copper rod thermally coupled to a copper support in contact with the heat tank (a hot plate whose temperature is controlled). The micro-TEG is located inside a sample holder thermally insulated from the hot plate, insuring the cold junctions to remain at room temperature. A hot plate temperature of 573 K yields to a temperature difference of about 240 K across the two junctions of the TEG. In this experiment, a part of the heat coming from the heat bath leaks in the surrounding air, inducing a loss of temperature gradient of about 60 K. It is worth noticing that a temperature difference of 240 K may generate an electrical power of about 45 µW ($V_{open} \sim 71\ mV$; $i \sim 1.3\ mA$ when $R_0 = R_L \sim 28\ \Omega$). Those values may open the field to many practical applications. It is also obvious to imagine how such micro-TEGs may produce much more usable electrical power when used in series or in parallel by conversion of the available surrounding hot sources which are generally wasted in the industries. Due to its small plain surface of ~ 6 cm² the micro-TEG may constitute the elementary brick of a bigger scale panel for which the elements could be connected in series or in parallel depending on the targeted applications. A panel constituted by 10×10 elements should therefore be able to generate an electrical power of 3.6mW when put in contact with a heat source of about 500 K.

5. Conclusion

In this work, a new thermoelectric microgenerator based on n-type $Bi_2Te_{2.7}Se_{0.3}$, and p-type $Bi_{0.5}Sb_{1.5}Te_3$ thin films is developed Films are deposited by sputtering on a 25 µm thick suspended membrane of polyimide. The specificity of this micro-TEG consists in its availability to convert high temperature differences (typically between 200 and 300 K) leading to maximum available electrical powers of few tens of µW. For our best prototypes, we experimentally generated a maximum power of 36 µW for a temperature difference of 206 K. In these steady state conditions, we obtained an open voltage of 64 mV, an internal resistance of 28 Ω, and a current in short circuit condition of 2.3 mA (the current in maximum power condition is 1.15 mA). Considering the entire surface on which the temperature difference is converted, the maximum power that has been measured experimentally reaches 14.2 µW/cm^2. This relatively high generated power is obtained in steady state conditions without the need to cool the cold bath (cold junctions), which is another particularity of this micro-TEG compared to devices in cross-plane configuration.

Another particularity of our micro-TEG is its ability to capture thermal power at the center of the device by direct thermal and mechanical contacts with surrounding heat baths. The flexibility and elasticity of the polyimide membrane insure a good thermal contact at the level of the central junction of the device. The adequation between versatility in heat harvesting and high-power generation opens the way to plenty of new applications.

Acknowlegments:

The authors want to gratefully thank E. André with whom we initiated these developments. We also thank the different technological pole of the Institut Néel for mechanical and thermal development. We also acknowledge the CNRS for financial support across its ''Pré-maturation'' program.

References :

[1] Venkatasubramanian R., Siivola E., Colpitts T., O'Quinn B.. Thin-film thermoelectric devices with high room-temperature figures of merit. Nature 2001;413:593-602.

[2] Harman T.C., Taylor P.J., Walsh M.P., Laforge B.E. Quantum dot superlattice thermoelectric materials and devices. Science 2002; 297:2229-2232.

[3] Chowdhury I., Prasher R., Lofgreen K., Chrysler G., Narasimhan S., Mahajan R.,Koester D., Alley R., Venkatasubramanian R.. On-chip cooling by superlattice-based thin-film thermoelectrics. Nat. Nanotech. 2009;4:235-238.

[4] Bulman G., Barletta P., Lewis J., Baldasaro N., Manno M., Bar-Cohen A., Yang B.. Superlattice-based thin-film thermoelectric modules with high cooling fluxes. Nat. Commun. 2016 ;7 :1030-1036.

[5] Harb A. Energy harvesting: State-of-the-art. Renew. Energy 2011; 36:2641.

[6] Vullers R.J.M., Van Schaijk R., Doms I., Van Hoof C., Mertens R., Micropower energy harvesting. Solid-State Electron. 2009;53:684.

[7] Madan D., Wang Z., Chen A., Wright P.K., Evans J.W. High-Performance Dispenser Printed MA p-Type Bi0.5Sb1.5Te3 Flexible Thermoelectric Generators for Powering Wireless Sensor Networks. Appl. Mater. Interfaces 2013;5:11872–11876.

[8] Kim S.J., Lee H.E., Choi H., Kim Y., We J.H., Shin J.S., Lee K.J., Cho B.J. High-Performance Flexible,Thermoelectric Power Generator Using Laser Multiscanning Lift-Off Process. ACS Nano 2016;10:10851–10857.

[9] Kim S.I., Lee K.H., Mun H.A., Kim H.S., Hwang S.W., Roh J.W., Yang D.J., Shin W.H., Li X.S., Lee Y.H., Snyder G.J., Kim S.W.. Thermoelectrics. Dense dislocation arrays embedded in grain boundaries for high-performance bulk thermoelectrics. Science 2015;348:109-114.

[10] Mzerd A., Sayah D., Tedenac J.C., Boyer A., Crystal growth and sticking coefficient of Bi2Te3 thin films on Si(111) substrate. J. Mater. Sci. Lett. 1994 ;13 :301.

[11] Boyer A., Cisse E., Properties of thin film thermoelectric materials: application to sensors using the Seebeck effect. Mater. Sci. Eng. B 1992 ;13 :103.

[12] Mu X., Zhou H.Y., He D.Q., Zhao W.Y., Wei P., Zhu W.T., Nie X.L., Liu H.J., Zhang Q.J.. Enhanced electrical properties of stoichiometric Bi0.5Sb1.5Te3 film with high-crystallinity via layer-by-layer in-situ Growth. Nano Energy 2017 ; 33 :55-64.

[13] Bourgault D., Giroud Garampon C., Caillault N., Carbone L., Aymami J.A., Thermoelectric properties of n-type Bi2Te2.7Se0.3 and p-type Bi0.5Sb1.5Te3 thin films deposited by direct current magnetron sputtering. Thin Solid Films 2008;516:8579-8583.

[14] Jeon S.J., Jeon H., Na S., Kang S.D., Lyeo H.K., Hyun S., Lee H.J.. Microstructure evolution of sputtered BiSb–Te thermoelectric films during post-annealing and its effects on the thermoelectric properties. J. Alloy Compd. 2013;553:343-349.

[15] Kim D., Byon E., Lee G-H., Cho S. Effect of deposition temperature on the structural and thermoelectric properties of bismuth telluride thin films grown by co-sputtering. Thin Solid Films 2006; 510:148.

[16,] Takashiri M., Tanaka S., Miyazaki K., Tsukamoto H.. Cross-plane thermal conductivity of highly oriented nanocrystalline bismuth antimony telluride thin films. J. Alloy. Compd. 2010;490:L44-L47.

[17] Makala R.S., Jagannadham K., Sales B.C., Wang H., Microstructure and Thermoelectric Properties of p-Type Bi0.5Sb1.5Te3 and n-Type Bi2Te2.7Se0.3 Films Deposited by Pulsed Laser Ablation.Mater. Res. Soc. Symp. Proc. 2002;691G8.4.

[18] Dauscher A., Thomy A., Scherrer H. Pulsed laser deposition of Bi2Te3 thin films. Thin Solid Films 1996;280:61-66.

[19] Giani A., Pascal-Delannoy F., Boyer A., Foucaran A., Gschwind M., Ancey P. Elaboration of Bi2Te3 by metal organic chemical vapor deposition. Thin Solid Films 1997; 303:1-3.

[20] Lin J.R., Snyder G.J., Huang C.K., Herman J.A., Ryan M.A., Fleurial J.P. Thermoelectric microdevice fabrication process and evaluation at the Jet Propulsion Laboratory (JPL). Proceedings of the 21st International Conference on Thermoelectricity, Long Beach CA, USA 2002;25-29:535.

[21] Del Fari D., Diliberto S., Boulanger C., Lecuire J.M. Étude électrochimique des systèmes binaires et ternaire engageant les éléments bismuth, antimoine et tellure. J. Phys. IV 2004 ;122 :53-58.

[22] Golgovici F., Cojocaru A., Anicai L., Visan T. Surface characterization of BiSbTe thermoelectric films electrodeposited from chlorides aqueous solutions and choline chloride based ionic liquids. Mater. Chem. Phys. 2011 ;126 :700-706.

[23] Murmu P., Shettigar A., Chong S., Liu Z., Goodacre D., Jovic V., Mori T., Smith K., Kennedy J. Role of phase separation in nanocomposite indium-tin-oxide films for transparent thermoelectric application,. Journal of Materiomics 2021;7: 612-620.

[24] Kennedy J., Murmu P., Kumar P., Ramanath G., Multifold enhancements in thermoelectric power factor in isovalent sulfur doped bismuth antimony telluride films. Materials Research Bulletin 2021;142:111426-111431.

[25] Huesgen T., Woias P., Kockmann N. Design and fabrication of MEMS thermoelectric generators with high temperature efficiency. Sens. Actuators A 2008;145–146:423-429.

[26] Van Toan, N., Tuoi, T.T.K., Ono, T., Thermoelectric generators for heat harvesting: From material synthesis to device fabrication. Energy Convers. Management 2020;225:113442.

[27] Davila D., Tarancon A., Calaza C., Salleras M., Fernandez-Regulez M., San Paulo A.,Fonseca L. Monolithically integrated thermoelectric energy harvester based on silicon nanowire arrays for powering micro/nanodevices. Nano Energy 2012 ;1 :812–819.

[28] Perez-Marin A.P., Lopeandia A.F., Abad L., Ferrando-Villaba P., Garcia G.,Lopez A.M., Munoz-Pascual F.X., Rodriguez-Viejo J., Micropower thermoelectric generator from thin Si membranes. Nano Energy 2014 ;4 :73–80.

[29] Yuan Z., Ziouche K., Bougrioua Z., Lejeune P., Lasri T., Leclercq D. A planar micro thermoelectric generator with high thermal resistance. Sens. Actuators A 2015 ;130221 :67–76.

[30] Tainoff D., Proudhom A., Tur C., Crozes T., Dufresnes S., Dumont S., Bourgault D., Bourgeois O. Network of thermoelectric nanogenerators for low power energy harvesting. Nano Energy 2019 ; 57 :804–810.

[31] Bourgault D., Garampon C.G., Caillault N., Carbone L. Thermoelectrical devices based on bismuth-telluride thin films deposited by direct current magnetron sputtering process. Sens. Actuators A 2018 ;273 :84–89.

[32] Nakamura Y., Isogawa M., Ueda T., Yamasaka S., Matsui H., Kikkawa J., Ikeuchi S.,Oyake T., Hori T., Shiomi J., Sakai A., Anomalous reduction of thermal conductivity in coherent nanocrystal architecture for silicon thermoelectric material. Nano Energy 2015;12:845–851.

[33] Sakata M., Hori T., Oyake T., Maire J., Nomura M., Shiomi J. Tuning thermal conductance across sintered silicon interface by local nanostructures. Nano Energy 2015 ;13 :601–608.

[34] Pennelli G. Review of nanostructured devices for thermoelectric applications. J. Nanotechnol. 2014 ;5:1268-1284.

[35] Champier D. Thermoelectric generators: A review of applications. Energy Convers. Management 2017;140:167-181.

[36] Directional Thermal diffusion realizing inorganic Sb2Te3/Te hybrid thin films with high thermoelectric performance and flexibility, Advanced Functional Materials, 2022; 1-9:2207903.

[37] Novel thermal diffusion temperature engineering leading to high thermoelectric performance in Bi2Te3-based flexible thin-films, Advanced Science, 2022; 5 : 2103547.

[38] Madan D., Wang Z., Wright P.K., Evans J.W. Printed flexible thermoelectric generators for use on low levels of waste heat. Appl. Energy 2015;156:587–592.

[39] Shi Y., Lü X., Xiang Q., Li J., Shao X., Bao W., Stretchable thermoelectric generator for wearable power source and temperature detection applications. Energy Convers. Management 2022;253:115167.

[40] Choi H., Kim Y.J., Kim C.S., Yang H.M., Oh M.W., Cho B.J. Enhancement of reproducibility and reliability in a high-performance flexible thermoelectric generator using screen-printed materials. Nano Energy 2018;46:39–44.

[41] Shin S., Kumar R., Roh J.W., Ko D.S., Kim H.S., Kim S.I., Yin L., Schlossberg S.M., Cui S., You J.M.,Kwon S, Zheng J, Wang J, Chen R. High-Performance Screen-Printed Thermoelectric Films on Fabrics. Sci. Rep. 2017;7:1–9.

[42] Wei Zhu W., Deng Y., Gao M., Wang Y, Hierarchical Bi–Te based flexible thin-film solar thermoelectric generator with light sensing feature. Energy Convers. Management 2015;106:1192–1200.

[43] Qing S., Rezaniac A., Rosendahl L. A., Enkeshafid A. A., Goua X. Characteristics and parametric analysis of a novel flexible ink-based thermoelectric generator for human body sensor. Energy Convers. Management 2018;156:655-665.

[44] Hsiao C., Wu Y. Fabrication of flexible thin-film thermoelectric generators. J. Chin. Inst. Eng. 2011;34:809-816.

[45] Trung N., Van Toan N. , Ono T. Fabrication of π-type flexible thermoelectric generators using an electrochemical deposition method for thermal energy harvesting applications at room temperature. J. Micromech. Microeng. 2017;27: 125006-9.

[46] Lu Z., Layani M., Zhao X., Tan L.P., Sun T., Fan S., Yan Q., Magdassi S., Hng H.H. Fabrication of flexible thermoelectric thin film devices by inkjet printing. Small 2014;10:3551–3554.

[47] Du Y., Xu J., Paul B., Eklund P., Flexible thermoelectric materials and devices. Applied Materials Today 2018; 12:366-388.

[48] Kato K., Hatazoka Y., Hashiwagi M., Hagino H., Adachi C., Miyazaki K. Fabrication of a Flexible Bismuth Telluride Power Generation Module Using Microporous Polyimide Films as Substrates, Journ. Electron. Mater. 2014;43:1733.

[49] Zhao L.D., Lo S.H., Zhang Y., Sun H., Tan G., Uher C., Wolverton C., Dravid V.P., Kanatzidis M.G. Ultralow thermal conductivity and high thermoelectric figure of merit in SnSe crystal. Nature 2014;508:373-377.

[50] Hinterleitner B., Knapp I., Poneder M., Shi Y., Müller H., Eguchi G., Eisenmenger-Sittner C., Stöger-Pollach M., Kakefuda Y., Kawamoto N., Guo Q., Baba T., Mori T., Ullah S., Chen X.-Q., Bauer E. Thermoelectric performance of a metastable thin-film Heusler alloy. Nature 2019;576:85.

[51] Bourgault D., Schaechner B., Giroud Garampon C., Crozes T., Caillault N., Carbone L. Transport properties of thermoelectric Bi0.5Sb1.5Te3 and Bi2Te2.7Se0.3 thin films. Journ. Alloys Compd. 2014;598:79.

[52] Thèse Giroud Garampon. Réalisation et étude des propriétés thermoélectriques de couches minces et nanofils de types Bi2-XSbxTe3 et Bi2Te3-xSex. 2011.

[53] Zhu W., Deng Y., Cao L. Light-concentrated solar generator and sensor based on flexible thin-film thermoelectric device. Nano Energy 2017; 34: 463-471.

[54] Mu X., Zhou H., He D., Zhao W., Wei P., Zhu W., Nie X., Liu H., Zhang Q. Enhanced electrical properties of stoichiometric Bi0.5Sb1.5Te3 film with high-crystallinity via layer-by-layer in-situ Growth, Nano Energy 2017; 33 : 55-64.
[55] Somdock N., Kianwimol S., Harnwunggmoung A., Sakulkalavek A., Sakdanuphab R. Simultaneous stoichiometric composition and highly (00l) orientation of flexible Bi2Te3thin films via optimising the DC magnetron sputter-deposition process. J. Alloys Comp. 2019;773 :78-85.